Broadband classification and statistics of echoes from aggregations of fish measured by long-range, mid-frequency sonar

Benjamin A. JonesTimothy K. StantonJohn A. ColosiRoger C. Gauss and Joseph M. FialkowskiJ. Michael Jech

Citation: The Journal of the Acoustical Society of America **141**, 4354 (2017); doi: 10.1121/1.4983446
View online: http://dx.doi.org/10.1121/1.4983446
View Table of Contents: http://asa.scitation.org/toc/jas/141/6
Published by the Acoustical Society of America

Broadband classification and statistics of echoes from aggregations of fish measured by long-range, mid-frequency sonar

Benjamin A. Jones[a)]
Office of the Oceanographer of the Navy, 2000 Navy Pentagon, Washington, DC 20350, USA

Timothy K. Stanton
Department of Applied Ocean Physics and Engineering, Woods Hole Oceanographic Institution, MS #11, Woods Hole, Massachusetts 02543, USA

John A. Colosi
Oceanography Department, Naval Postgraduate School, 833 Dyer Road, Monterey, California 93943, USA

Roger C. Gauss and Joseph M. Fialkowski
Code 7164, Naval Research Laboratory, 4555 Overlook Avenue SW, Washington, DC 20375, USA

J. Michael Jech
NOAA Northeast Fisheries Science Center, 166 Water Street, Woods Hole, Massachusetts 02543, USA

(Received 28 August 2016; revised 8 March 2017; accepted 1 May 2017; published online 13 June 2017)

For horizontal-looking sonar systems operating at mid-frequencies (1–10 kHz), scattering by fish with resonant gas-filled swimbladders can dominate seafloor and surface reverberation at long-ranges (i.e., distances much greater than the water depth). This source of scattering, which can be difficult to distinguish from other sources of scattering in the water column or at the boundaries, can add spatio-temporal variability to an already complex acoustic record. Sparsely distributed, spatially compact fish aggregations were measured in the Gulf of Maine using a long-range broadband sonar with continuous spectral coverage from 1.5 to 5 kHz. Observed echoes, that are at least 15 decibels above background levels in the horizontal-looking sonar data, are classified spectrally by the resonance features as due to swimbladder-bearing fish. Contemporaneous multi-frequency echosounder measurements (18, 38, and 120 kHz) and net samples are used in conjunction with physics-based acoustic models to validate this approach. Furthermore, the fish aggregations are statistically characterized in the long-range data by highly non-Rayleigh distributions of the echo magnitudes. These distributions are accurately predicted by a computationally efficient, physics-based model. The model accounts for beam-pattern and waveguide effects as well as the scattering response of aggregations of fish. © *2017 Acoustical Society of America*.
[http://dx.doi.org/10.1121/1.4983446]

[BTH] Pages: 4354–4371

I. INTRODUCTION

Fish have been detected by horizontal-looking sonar systems at ranges up to 60 km since the late 1960s.[1–4] Such long-range systems, which typically have detection ranges much greater than the water depth, have distinct advantages over conventional downward-looking echosounders as they can rapidly capture the high degree of spatio-temporal variability of fish over large areas. However, only a few studies have attempted to quantify distributions of fish using long-range systems.[4–8] This is due, in part, to the difficulty in distinguishing between echoes from fish and from other sources of scattering as well as challenges associated with rigorously accounting for ocean waveguide effects. Similar complications affect active sonar systems when trying to detect or classify other scatterers of interest where fish may be an unwanted source of uncertainty. This latter case has led to recent efforts to quantify the impacts of biologics as a source of interference on some mid-frequency systems.[9–11] A major limitation in most systems, to date, is that the sonars are narrowband—that is, they use signals whose bandwidth is about 10% of the center frequency. These narrowband systems have limited capability to classify scatterers in the spectral domain where unique scattering properties exist. For example, fish with a gas-bearing swimbladder have a strong resonance peak at a frequency that depends upon the size, species, and depth of the fish. Narrowband systems that do not have adequate spectral coverage or frequency resolution are subject to poor characterization or even aliasing of this resonance feature.

This limitation, associated with previous narrowband long-range systems, is addressed through the use of a recently developed horizontal-looking sonar system whose signals are broadband and continuously span the frequencies over a range of 1.5–9.5 kHz.[8] A sub-band of this system (1.5–5 kHz), optimized for the observed environment, is

a)Electronic mail: benjamin.a.jones@navy.mil

 0001-4966/2017/141(6)/4354/18/$30.00

exploited in an ocean experiment in which echoes exhibit key spectral features uniquely characteristic of the acoustic resonance of fish swimbladders. These data, consisting of observations of sparse, compact aggregations of scatterers, on the order of hundreds of meters in length, are complemented by biological sampling and downward-looking echosounder measurements collected during the same experiment. Analysis of the horizontal measurements in the time domain reveal that the echo magnitudes have strongly non-Rayleigh distributions that are well-modeled by a physics-based statistical model which accounts for sonar system parameters and waveguide effects.

This research applies, in part, to the use of sonar to survey fish for purposes of both species classification and abundance estimation. There have been a number of studies using horizontal-looking narrowband systems (i.e., sonar with spectral coverage of ~5%–15% of the center frequency) to measure fish populations involving both commercial and scientific systems.[5,6,12] Fisheries applications (i.e., fish finding sonar) typically involve ranges of hundreds of meters to 1 km,[13,14] but can extend to 30–50 km.[2,15] A strength of these systems is that they can be used to rapidly survey large volumes of water enabling researchers to measure fish populations even when the fish are sparsely distributed (i.e., separated in space more widely than the typical beamwidth of a downward looking echosounder). However, complications arise when trying to interpret echoes from widely distributed sources because complementary data are difficult to obtain. For example, it is not practical to continuously or uniformly sample a large region with trawls. In addition, the combination of a narrow beam and a refractive waveguide can lead to a highly non-uniform distribution of acoustic energy in the water column[16] potentially causing significant underestimates in abundance calculations. Furthermore, since the depths of the fish are generally not known, it can be difficult to discriminate between seafloor reverberation and scatterers in the water column. Spectral signatures may be exploited; however, narrowband systems that use only one or even several discrete frequencies may be unable to take advantage of this information. The challenge is further complicated by the dynamic behavior of fish and the depth dependency of the swimbladder resonance. These effects can, potentially, induce large errors in measurements by systems incapable of near-simultaneous measurements across the relevant frequency band. For example, a shift in the resonance peak, due to the fish changing depths as part of their diurnal vertical migration, could be wrongly interpreted as a change in abundance.

Fortunately, the spectral characteristics of fish can be fully exploited when using a broadband system.[17–19] For example, the gaseous swimbladder-bearing fish, observed in this experiment, produced a resonance in or near the frequency range of the employed sonar (1.5–5 kHz). Due to the strength of the resonance, the fish echoes could be observed above the background reverberation. Furthermore, they could be discriminated from other strong sources of scattering such as the seafloor because of the unique spectral characteristics of the resonance.

Another application of this research involves the degradation of performance of active sonar systems due to the presence of fish when they are not the scatterer of interest. Sonar systems that transmit broadband signals and receive echoes on high-resolution arrays benefit from a high degree of temporal and spatial resolution particularly when match-filtered (i.e., correlated with the transmitted signal). However, echoes from environmental sources such as fish can both mask real echoes of interest and overload the sonar operator with false alarms. To help reduce the false alarm rate, several studies have been conducted to devise signal-processing strategies to separate real from false targets based on temporal-spectral characteristics[20,21] and statistical analyses of the received time series.[9,10,22] In these latter studies sonar "clutter" is characterized by echoes that exceed a given threshold above the mean background level (sum of reverberation and noise), and are similar to those being measured. For example, since the temporal extent of an echo is related to the size of the scattering volume (coupled with propagation effects—e.g., see Ref. 23), compact aggregations of scatterers that are of target scale are more likely to present a false alarm case to a sonar operator.

An important characteristic of clutter is the statistical distribution of the echo envelopes—the magnitudes of the received complex signal. Specifically, a "heavy-tailed" probability density function (PDF), where the high amplitude portion of the distribution is elevated above a Rayleigh distribution, indicates a higher probability of false alarm. There are several contributing factors which can lead to this type of non-Rayleigh distribution. In a direct path case it has been shown that the key factors are the number of scatterers in the beam, the source and receiver beampatterns, and the scattering response.[24] However, there are no studies to date examining the effects of these physical factors on statistics of echoes from scatterers in the water column observed at long ranges. As will be shown in this study, echoes from sparsely distributed, compact aggregations of fish are observed to have both the spatial structure and statistical characteristic of clutter as described above.

Two experiments were conducted in the Gulf of Maine in 2010 and 2011 which included long-range (up to 12 km) mid-frequency active sonar measurements. This set of experiments is unique in that the long-range acoustic measurements are broadband, with frequencies that continuously span the range 1.5–9.5 kHz. This broadband capability enables simultaneous detection and classification of fish aggregations by exploiting the swimbladder resonance. These measurements are complemented with downward-looking multi-frequency measurements and fish trawls from a second vessel. Of interest to this study are those measurements taken near Franklin Swell in 2011 in which sparse, compact scatterers were observed in the long-range, horizontal sonar data. Fish trawls in this area sampled mixed species of swimbladder-bearing fish. Key results include the spectral classification of sparsely distributed aggregations of swimbladder-bearing fish with normalized echo levels at least 15 dB above the seafloor-dominated background reverberation levels. Furthermore, these echoes are characterized by highly non-Rayleigh echo statistics. The echo-envelope distributions are well modeled by a computationally efficient

calculation that accounts for waveguide effects and beampatterns of the source and receiver.[16]

This article is organized as follows: Section II describes the 2011 Gulf of Maine experiment. Section III describes the acoustic models used to predict frequency-dependent scattering by fish swimbladders, propagation of the long-range sonar signal, and distributions of the magnitudes of echoes from aggregations of fish. Section IV details the steps used to process and analyze the long-range acoustic data. Section V describes the results in four sections: (1) downward-looking echosounder data, (2) biological sampling (fish trawls), (3) spectral classification of the long-range echoes, and (4) statistical characterization of the long-range echoes. Finally, Secs. VI and VII are the discussion and concluding remarks, respectively.

II. GULF OF MAINE EXPERIMENT

A collaborative experiment between Woods Hole Oceanographic Institution (WHOI), the Naval Research Laboratory (NRL), and the National Oceanic and Atmospheric Administration's Northeast Fisheries Science Center (NOAA-NEFSC) was conducted in September of 2011 to measure the spatial distribution and clutter characteristics of aggregations of fish in the Gulf of Maine. The experiment was conducted from two research vessels, the Fisheries Research Vessel (FRV) *Delaware II* (NOAA-NEFSC team) and the Research Vessel (RV) *Oceanus* (WHOI and NRL teams). The experiment was unique in that: (1) the measurements were taken from a long-range, horizontal-looking system that used broadband pulses whose frequency spectrum continuously spanned a wide range of frequencies allowing resonance classification of swimbladder-bearing fish, and (2) the long-range acoustic data were complemented by measurements from a narrowband, downward-looking echosounder and net samples of fish. Additionally, this study is complemented by previous measurements taken in the same region using a downward-looking, broadband (1–6 kHz) system that largely overlaps with the frequency band used in this study. Those measurements, collected during a series of experiments,[17–19] provide empirical validation of swimbladder-resonance characteristics observed in this experiment.

Of particular interest to this analysis are measurements of compact aggregations of fish from the horizontal-looking, long-range sonar in the vicinity of Franklin Swell (Fig. 1). Data analyzed in this paper were derived from long-range (i.e., 1–12 km), acoustic measurements made on September 11, 2011. This data set was chosen due to environmental conditions that permitted long-range reception of high signal-to-noise ratio (SNR) echoes from the scatterers in the water column. Additionally, the analysis focuses on a short period of time to ensure stationarity of the data. However, echoes with qualitatively similar spectral and temporal characteristics were observed at other times during this experiment and in previous experiments employing this broadband, long-range system.[8]

Considering the large volume of water surveyed nearly instantaneously with the long-range sonar and given that the data of interest were from compact, mobile aggregations of fish at unknown depths, one-for-one comparison between the sonar data and secondary measurements, such as local echosounder data or trawls, is not feasible with current

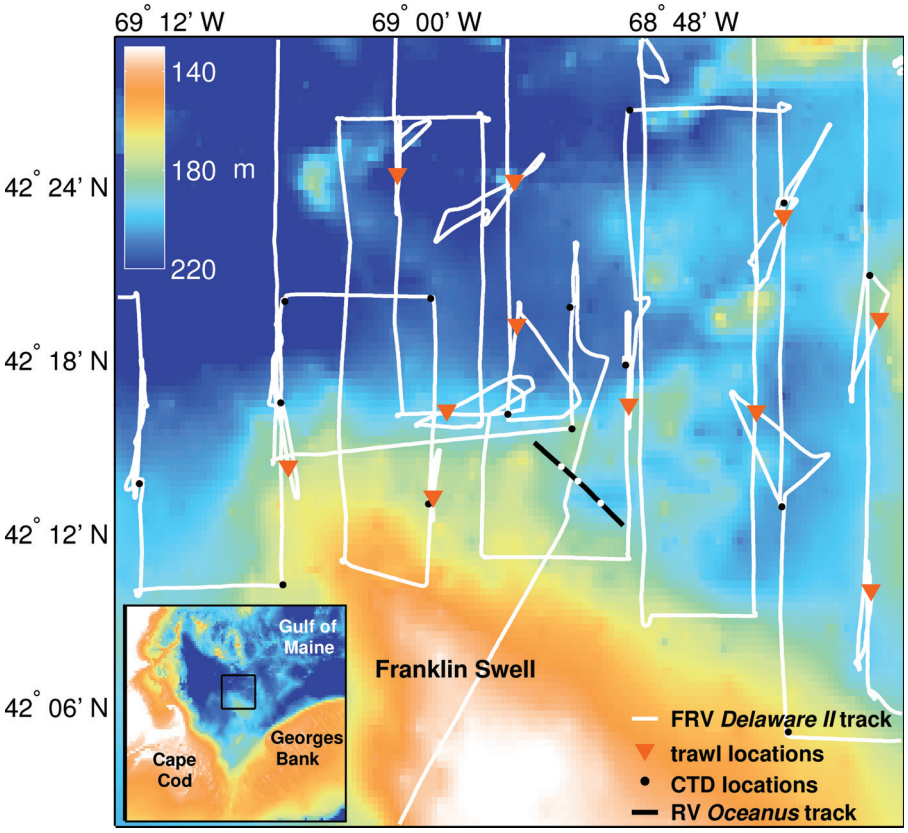

FIG. 1. Map showing bathymetry and cruise tracks of RV *Oceanus* from 2221 to 2359Z on September 11, 2011 (black line) and FRV *Delaware II* from September 11–15, 2011 (white lines). White circles along *Oceanus* track represent the midpoints of tracks where data sets A/B, C, and D were collected (northwest to southeast, respectively). Trawl location along the *Delaware II* track are also shown (orange triangles). Black dots represent locations of CTD casts that were used in this analysis. Inset shows small-scale map of Gulf of Maine with region of interest outlined in black.

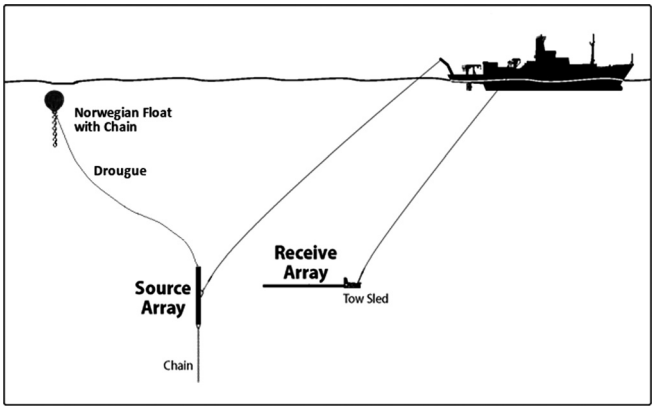

FIG. 2. Deployed configuration of NRL long-range, horizontal-looking sonar system (not to scale).

technology. In order to address this issue, the area was characterized extensively from 9 to 15 September 2011, through repeated surveys using downward-looking echosounders and trawls over a range of conditions: day and night and over the full range of depths in the vicinity of the Franklin Swell area (Fig. 1). This significant database, in combination with modeling of acoustic propagation and scattering, is used to help verify the interpretation of the sonar data in terms of the various sources of scattering that are present.

A. Long-range, horizontal-looking sonar system (NRL)

The NRL sonar system consisted of a 10-element, broadband (1.5–9.5 kHz), vertical line array (VLA) source and a 32-element horizontal line array (HLA) receiver.[8] Both were towed concurrently at 1.5 m/s aft of the RV *Oceanus*, with the source VLA deployed from the aft A-frame and the receiver HLA deployed amidships (Fig. 2). Typical separation between the two systems was ∼30 m. Initially, signals spanning the entire frequency range were transmitted before switching to sub-bands with a higher SNR to exploit resonances identified in the observed echoes.

Echoes from two linear frequency modulated (LFM) pulsed waveforms are analyzed: LFM1—a signal with a bandwidth, w, of 700 Hz centered at 3750 Hz, and LFM2—a 3.5-kHz bandwidth signal centered at 3250 Hz (Table I). These waveforms were transmitted in sequence with two other signals with a 20-s delay between each transmission giving a total cycle time of 80 s between transmissions of a given waveform. Echoes analyzed in this analysis come from four data sets (Sets A, B, C, and D) acquired during 2227–2350Z (1827–1950L—local) on September 11, 2011, in the vicinity of Franklin Swell (Fig. 1). During this period the source and receiver depths were centered at 48 and 38 m, respectively.

TABLE I. Parameters of employed signals including signal type, bandwidth, w, start frequency, f_0, end frequency, f_1, and pulse length, T_P. A 10% Tukey window is applied to the transmit waveforms resulting in tapering of 175-Hz band on each side of the spectra.

Signal	Signal type	w (Hz)	f_0 (Hz)	f_1 (Hz)	T_P (s)
LFM1	LFM	700	3400	4100	2
LFM2	LFM	3500	1500	5000	2

B. Downward-looking narrowband echosounder (NOAA-NEFSC)

A hull-mounted, downward-looking Simrad EK60 scientific echosounder collected multi-frequency (18, 38, 120 kHz) acoustic data continuously aboard the FRV *Delaware II*. These echosounder data were processed by the NEFSC team using a combination of manual analysis and automated classification and detection algorithms to identify schools of fish with gas-filled swimbladders, classify these aggregations into Atlantic herring (*Clupea harengus*) and non-herring schools, and extract parameters for each school (e.g., school depth, school length, school thickness, and volume backscattering strength).[25,26]

C. Biological sampling (NOAA-NEFFC)

Trawl hauls were conducted from the FRV *Delaware II* using a polytron mid-water rope trawl with a mouth opening of 35 m, horizontally, and 15 m vertically. The times, depths, and durations at which the trawl was deployed were based on real-time data from the echosounder that indicated the presence of fish. Typical tow rates were 1.8 m/s. Twelve trawls were conducted between the 11th and 15th of September 2011, within 25 km of the RV *Oceanus* ship track of September 11, 2011 (Fig. 1). For one haul, depths were not recorded on the temperature-depth recorders attached to the headrope and footrope, so only eleven trawl samples were used in this analysis. Trawl catches were processed identifying the number, weight, species composition, and fork length, L_{FL}, of fish caught. In addition, the deployment times, tow duration, depths, and geographic locations of the start and end of each tow were recorded for each trawl deployment.

D. Environmental characterization

The long-range acoustic data were collected on September 11, 2011, in the period between 2227–2350Z, which was during day and twilight hours (sunset at 2253Z; end of nautical twilight at 2354Z). During this period seas were slight with winds of 5 to 6 m/s from the south-southeast. The seafloor at Franklin Swell is primarily sand, with the slopes leading up to the swell consisting of a mixture of sand, silt and clay.[27]

Vertical profiles using conductivity, temperature, and depth (CTD) sensors were conducted from the FRV *Delaware II* using a Sea-Bird Electronics (SBE) model 19*plus*. To characterize the environment for acoustic propagation modeling, all of the 15 CTD measurements that were considered in this analysis were taken during the days of September 11–15, between the times of 1200–2359L, and within approximately 25 km of the RV Oceanus ship track of September 11, 2011 (Fig. 1). Measurements were made over a range of depths from the surface to a maximum depth of 227 m (Fig. 3). The thermocline shown in the temperature profile between 15 and 45 m indicates favorable conditions

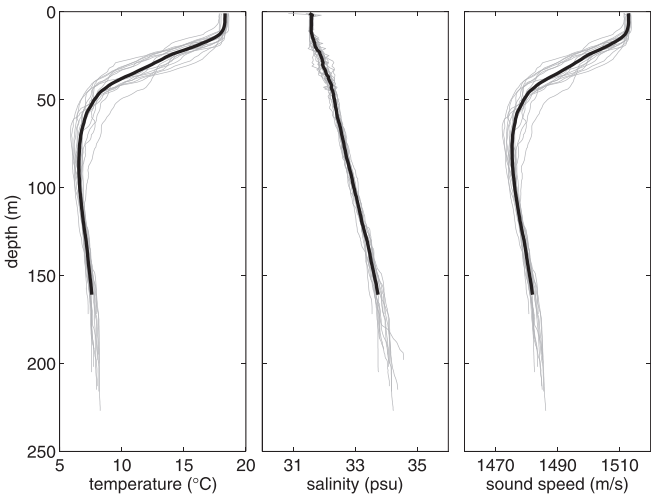

FIG. 3. Temperature, salinity, and sound-speed profiles derived from CTD casts taken from FRV *Delaware II* during times of 1200 to 2359 local between the 11th and the 15th of September 2011. Mean profiles are shown in thick black curves.

for diffuse internal waves which are generally present in a stratified water column with tidal forcing.

III. ACOUSTIC MODELS

Three separate acoustic models are used independently to compare with the observed long-range acoustic data. The first is a spectral model that predicts the frequency-dependent backscattering levels of mixed assemblages of fish based on the species and length-distribution of fish in the trawl catches. This model is based, predominantly, on the Love resonant-swimbladder-scattering model described in the Appendix. The second is a range-dependent propagation model used to predict transmission loss in the presence of random, diffuse internal wave fields. Finally, PDFs of echo magnitudes are predicted using a continuous wave (CW) phasor-summation model that accounts for sonar system characteristics, waveguide effects, and the scattering response of resonant fish schools.[16] Probability density functions are calculated using a Monte-Carlo method in which the location of the fish aggregation within the beam, the scattering response, and noise are random variables.

A. Volume backscattering by aggregations of fish

Target strength, TS, is the logarithmic measure of a backscattered signal in dB relative to square meters (dB re 1 m^2) and can be expressed as

$$\mathrm{TS} = 10\log_{10}(\sigma_{\mathrm{bs}}), \tag{1}$$

where $\sigma_{\mathrm{bs}} = |f_{\mathrm{bs}}|^2$ is the differential backscattering cross section in m^2 and f_{bs} is the backscattering amplitude in m. The average volume backscattering strength of a mixed aggregation of scatterers with an average differential backscattering cross section of $\bar{\sigma}_{\mathrm{bs}}$ and a numerical density, ρ_{s}, of scatterers per m^3 for each species is given in dB relative to m^{-1} (dB re $1\,m^{-1}$) as

$$\overline{S_V} = 10\log_{10}\left(\sum \rho_{\mathrm{s}}\bar{\sigma}_{\mathrm{bs}}\right), \tag{2}$$

where the sum is over the various species involved in the composition.

A resonance model for acoustic scattering by individual fish swimbladders has been widely used to model scattering by fish ensonified at frequencies with an acoustic wavelength much longer than the length of the swimbladder. This formulation, given by Nero *et al.* in a simplified form[28] and used to calculate σ_{bs}, is provided in the Appendix.

B. Acoustic propagation model

A parabolic equation (PE) model is used to calculate transmission loss of the long-range horizontal-looking sonar signal along transects where fish were observed in the data (parameters given in Table II). The PE formulation is based on the range-dependent acoustic model (RAM)[29] which has the capability of including range-dependent features of the shallow water environment. Specifically, the propagation model used here (described in detail in Ref. 16) incorporates internal-wave (IW) induced perturbations to the mean sound-speed field to capture the natural randomness of the ocean environment. Modeling of internal wave fields[30] is based on the mean observed sound speed profile (Fig. 3). Depth profiles of key derived parameters are shown in Fig. 4.

C. Numerical predictions of echo statistics—phasor summation method

PDFs of echo envelopes from water column scatterers at long ranges can be predicted using a numerically efficient Monte-Carlo method. This method, a simple phasor-summation formulation, is mathematically equivalent, in special cases, to the analytical Chu–Stanton model.[24]

TABLE II. Model parameters for acoustic propagation modeling.

Parameter	Value
Source parameters:	
source type	10-element VLA
element spacing (m)	0.248
source depth (m)	48
rms source level (dB)	observed[a]
center frequency (Hz)	3750
bandwidth (Hz)	100
Environmental parameters:	
bathymetry	USGS database (Ref. 44)
sound-speed profile	range-dependent[b]
seafloor type	database (Ref. 27)
IW displacement, ζ_0 (m)	2
IW buoyancy frequency, N_0 (cycles/h)	3
IW modes, $j_{\max}$	20
RAM parameters:	
frequency resolution (Hz)	1.69
range step (m)	1
depth step (m)	0.025
number of Padé terms	4

[a]Source level is derived from observed power levels applied to the elements.
[b]CTD-derived mean sound-speed profile perturbed by diffuse IWs (Ref. 45).

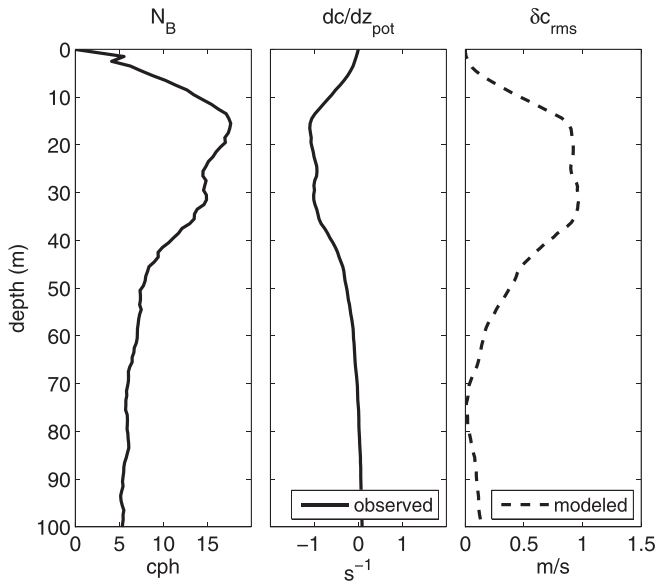

FIG. 4. Water column profiles associated with observed mean profile (thick black curves, Fig. 3) from Franklin Swell area in the Gulf of Maine from September 2011. Profiles shown are buoyancy frequency (left panel), the derivative of potential sound speed with depth (center panel), and modeled range-averaged, rms sound-speed perturbation (right panel).

Importantly, the Chu–Stanton model captures a key statistical effect whereby the echoes of scatterers, randomly located in a directional sonar beam, are modulated by the beampattern function producing a predictable distribution of echo envelopes. While this formulation was developed for direct path scattering by point scatterers, the Chu–Stanton theory has been applied to finite-length extended scatterers at long ranges by accounting for waveguide effects.[16] These effects include the attenuation of high-propagation-angle energy and the squaring of the one-way response due to reciprocity of forward and back-propagated acoustic paths. The term *finite-length extended scatterer* implies that the scattering volume is large compared with the correlation length of the incident pressure field, yet small enough to subtend an angle that can be approximated as a constant value. This approximation enables calculation of the azimuthally dependent beampattern without knowing the precise size of the scattering volume—in this case an aggregation of fish.

The phasor-summation model is compared with echo magnitude PDFs of aggregations of fish ensonified by a horizontal-looking directional sonar at various ranges. In each phasor-summation prediction 5×10^5 realizations are calculated in which a single, finite-length extended scatterer with a Rayleigh-distributed response (before beampattern effects) is randomly located in the main lobe of a directional sonar beam. Normalized PDFs were formed from histograms of the echo magnitudes normalized by the root mean square echo amplitude of the ensemble.

IV. DATA ANALYSIS METHODS

A. Beamforming and normalization

LFM1 and LFM2 data were beamformed azimuthally to form 33 Hamming-weighted, cosine-spaced beams with beams 1, 17, and 33 representing forward-endfire, broadside, and aft-endfire beams, respectively. Subsequently, the data were processed using a matched-filter followed by a split-window normalization.[22] This latter technique implements a sliding window in which a sample at the center of this window is normalized by the mean envelope in a window (the auxiliary band) separated, or *split*, by a small window (the guard band) that is centered on the sample and excluded from the mean normalization value. The resulting value at each sample, then, is a signal-to-reverberation ratio (SRR)—or the power ratio of the echo to the local reverberation-dominated background (including noise). In both the spectral and statistical analyses, normalized echoes, with SRRs of at least 15 dB, were identified in order to define time windows for extracting *unnormalized* echoes for further analysis.

B. Spectral analysis

The 3.5-kHz-bandwidth data corresponding to LFM2 transmissions of data sets A–D (Table III) were normalized using a guard band of $2/w = 5.71 \times 10^{-4}$ s, where w is the transmit waveform bandwidth, and an auxiliary band of 5.41×10^{-1} s. Time bins were then identified by centering a 2.67×10^{-1} s window, corresponding to a range extent of approximately 200 m, around echoes with SRRs of at least 15 dB. Echoes were grouped within given beams and transmission periods (Table III), and analyzed within range bins determined by two-way travel time. Mean spectra were formed from each data set by taking the Fourier transform of the matched-filtered data (before normalization) corresponding to those time bins, correcting for frequency-dependent source level and water-column attenuation, and then averaging over all echoes. A mean background level was determined from 2.67×10^{-1} s periods of beam-level data just prior to LFM2 transmissions for transmissions and beams corresponding to echoes used in the calculations of the mean spectra. Finally, a 6 dB SNR threshold was applied to each Fourier component of the mean spectra to reduce noise contamination.

TABLE III. Long-range acoustic data sets defined by time of transmission and range of receiver beams from which data were drawn.

Data set	Time period (UTC)	Ship track midpoint (deg)	Number of pings	Beam subset
A	22:40:54–22:58:14	42.24 N 68.90 W	14	15–25[a]
B	22:36:54–22:58:14	42.24 N 68.90 W	16	25–30[a]
C	22:58:14–23:16:54	42.23 N 68.88 W	15	20–30[a]
D	23:16:54–23:50:14	42.22 N 68.86 W	25	20–30[a]

[a]Beam 1 represents forward endfire and beam 33 represents aft endfire.

In order to assess the swimbladder-resonance features in the observed spectra, an average frequency-dependent, differential backscattering cross-section, $\bar{\sigma}_{bs}$, is calculated for each dominant fish species observed in the Franklin Swell region using the Love resonance model (described in Sec. III A). Effects of multiple scattering and resonance shifts have both been ignored as the observed fish schools do not meet the high packing density required to make these effects significant.[31] This model has been successfully used in a study using a downward-looking broadband system conducted in the same geographic region, same time of year, and at the same frequencies as in this experiment with the long-range, horizontal looking sonar system.[18] The $\bar{\sigma}_{bs}$ term for each species is weighted by the length distribution observed in the trawl hauls for that species. Finally, an average volume backscattering strength is calculated by weighting $\bar{\sigma}_{bs}$ with a relative numeric density for each species [Eq. (2)].

The data-model comparison is a two-step process. First, the model parameter for the depth of the fish is determined by fitting the modeled spectra, along the frequency axis, to the main resonance peak. Second, the relative densities of each contributing fish species are determined by a best fit of the predicted volume backscattering strength to the frequency dependent echo levels of the observed data.

C. Echo statistics

The 700-Hz-bandwidth data corresponding to LFM1 transmissions of data sets B–D were normalized using a guard band of 2.90×10^{-3} s, corresponding to $2/w$, and an auxiliary band of 5.41×10^{-1} s. Echoes were extracted from the unnormalized data that met the threshold criterion in the normalized data using 2.67×10^{-1} s sample windows centered on the sample with the peak level. Ensembles were formed within a given range bin (based on two-way travel time) where the ensemble is of echo envelopes, sampled across the temporal extent of the echo. PDFs were generated from histograms of these echo envelopes and normalized by the rms echo amplitude of the ensemble for comparison with theory.

A primary criterion when calculating statistics of the echoes is that the ensemble is formed from independent samples with a stationary mean. The primary assumption used here is that the environment is locally stationary (i.e., the statistics are stationary over the short period of time and narrow region in space). Echoes analyzed are limited to those arising from sonar transmissions covering a period of approximately 73 min when the echoes appear to be dominated by Atlantic herring (sets B–D, Table III). During this period it is assumed that the mean characteristics of the ocean (e.g., the mean sound speed profile) are constant. Furthermore, the echoes are grouped into 0.67-s bins, a period of two-way travel time corresponding to approximately 500 m of spatial extent. Due to the narrow time bin and the high selection threshold of 15 dB, which likely limits the echoes to those associated with scatterers in the energetic portion of the waveguide (i.e., not including the shadow zones), the transmission losses for the echoes are assumed constant across echoes within a given time bin.

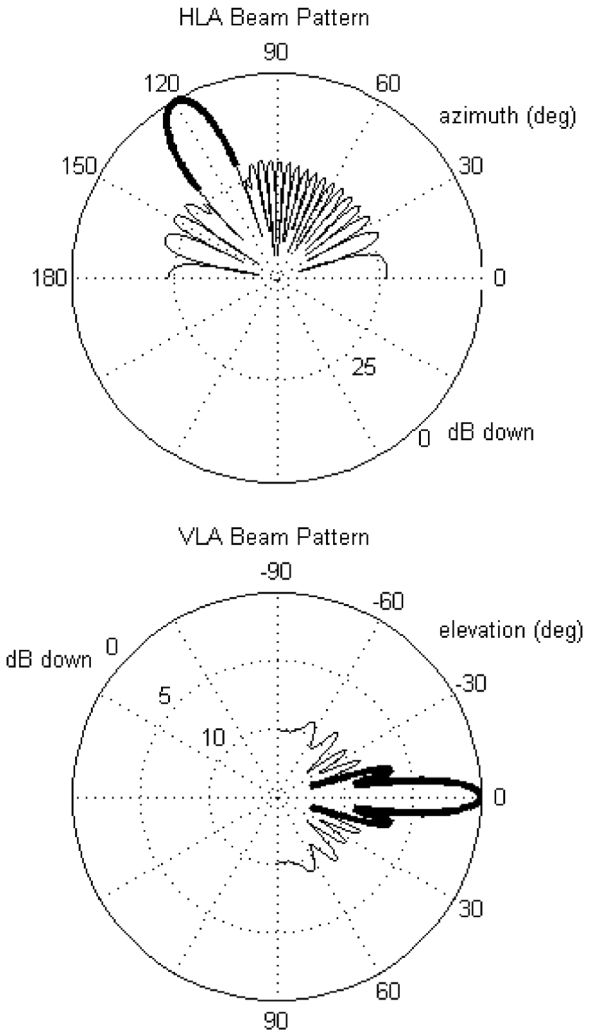

FIG. 5. Theoretical beampatterns in terms of pressure envelope at 3.75 kHz (black) for beam 25 of a shaded 32-element HLA (top panel) and an observed-level-weighted 10-element VLA (bottom panel). HLA shading is a Hamming window; while, VLA shading is based on average observed power drawn by VLA elements. Heavy black line is the angular extent of the location of scatterers within the beam used in the numerical phasor summation simulations (i.e., portion of main lobe above sidelobes for HLA, and main lobe and first side lobe for VLA).

Echoes are assumed to be independent from ping to ping based on the 80-s cycle time between transmissions. To ensure that samples from within a given echo were non-overlapping, the matched-filtered echo envelopes were sub-sampled at a spacing of 1.5×10^{-3} s, roughly the time resolution of the waveform (1.4×10^{-3} s). To determine if this sample spacing was sufficient to ensure independence of samples within an echo, the e-folding correlation time, τ_e, was calculated as $\langle R_{xx}(\tau_e) \rangle = R_0/e$, where R_{xx} is the autocorrelation function for each echo, R_0 is the maximum value at a delay time, $\tau = 0$, and the mean is calculated over all echoes in a given time bin. The resulting e-folding times for all bins, $\tau_e < 1.31 \times 10^{-3}$, was less than the sample spacing ensuring no correlation between samples.

In this analysis, theoretical predictions of echo PDFs are calculated using the phasor-summation method (see Sec. III C) at the center frequency of the transmitted waveform, 3750 Hz. In these calculations the scattering amplitudes are

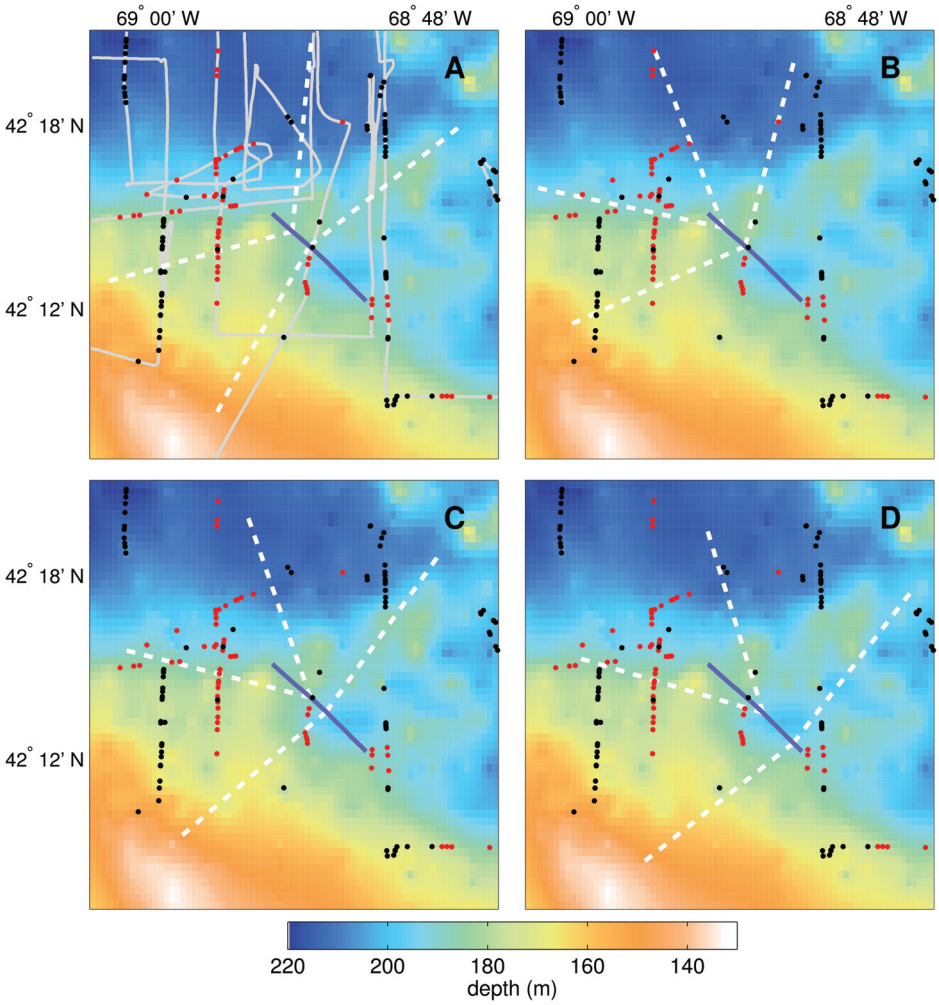

FIG. 6. Bathymetry and cruise track of RV *Oceanus* from 2221 to 2359Z on September 11, 2011 (blue lines) and portions of the FRV *Delaware II* from September 11–15, 2011 (grey lines—panel A). Locations of schools of herring (red) and non-herring (black), observed by downward-looking echosounder, are overlayed with maximum lateral extents of the −3 dB beam limits out to 12 km of the long-range, horizontal looking system on RV *Oceanus* (white dashed lines). These beam limits, with left-right ambiguity shown, correspond to beam-space analyzed in long-range horizontal measurements for sets A–D (see Table III).

modeled as a zero-mean complex Gaussian PDF, p_A, which corresponds to magnitudes of scattering responses that are Rayleigh distributed. The source beampattern in the vertical plane is calculated from a theoretical beampattern weighted by the mean observed power applied to the 10-element VLA over the range of frequencies in the waveform (Fig. 5). The elevation angle, ϕ, is limited in extent to account for waveguide effects, i.e., the sound is projected over a narrow range of angles in the vertical plane and centered about the horizontal direction. The exact values of ϕ used in these calculations were determined by fitting to the data. The receiver beampattern in the horizontal plane is derived from a theoretical beampattern for a 32-element, Hamming-weighted HLA corresponding to the median of the primary look directions for the observed fish echoes (beam 25, the forward-most beam analyzed in data set B and the center beam for data sets C and D). Predictions were made only for the main lobe (i.e., the source was modeled as having zero response for azimuthal angles outside the main lobe). This restriction accounts for selectivity of echoes from scatterers located within the main lobe of the acoustic beam imposed by the high SRR criterion. Finally, zero-mean, complex-Gaussian-distributed noise was added coherently to the phasor-summation result to account for interfering noise (both system and ambient) and reverberation not originating from fish in the observed data. The resultant signal, then, is $\hat{s}_1 = \hat{s} + \hat{n}$, where $\hat{s}$ is the complex pressure summed over N scatterers and $\hat{n}$ is the additive noise and reverberation. The latter was fit to the low amplitude portion of the PDFs in all cases.

V. RESULTS

A subset of the long-range acoustic data characterized by compact and spatially sparse scatterers is examined. To classify the echoes as originating from fish aggregations or from other sources, several contemporaneous acoustic and non-acoustic data sets were analyzed. A key limitation of the experiment was that one-for-one comparison between echoes from the long-range sonar and fish sampled was not possible. This limitation is due to the fact that the fish schools were not only small and mobile, but furthermore, their depths were unknown since depth cannot, generally, be resolved by a long-range sonar. In order to address this issue, fish were systematically sampled throughout the region during the same week as the long-range range acoustics experiment over a range of conditions, including both day and night and over the full range of depths. This provided a statistical basis for interpreting the long range sonar data in terms of the fish present. Fish samples and related data collected between September 11 and 15, 2011, within 25 km of the RV

Oceanus track of September 11, 2011, are presented. These data include downward-looking acoustic data, biological samples, and water-column profiles.

A. Characteristics of fish schools derived from downward-looking echosounder measurements

Fish echoes collected with the downward-looking echosounder on FRV *Delaware II* were analyzed to derive a variety of parameters pertaining to aggregations of fish in the vicinity of Franklin Swell. The data are divided into Atlantic herring and non-herring schools with each aggregation analyzed according to their depth, length, thickness, and volume backscattering strength. Figure 6 shows the locations of the observed fish aggregations in relation to the long-range acoustic data collection. The beam-spaces considered in data sets A–D are overlaid with locations of herring and non-herring schools observed by the echosounder.

Distributions of the depth and altitude (i.e., height above the seafloor) of fish schools are shown for periods of day, dusk (1 h prior to sunset to the end of nautical twilight), night, and dawn (beginning of nautical twilight to 1 h post-sunrise) in Fig. 7—herring and Fig. 8—non-herring. The depth distribution of Atlantic herring is narrowly distributed around 180 m during the day, rising approximately 15 m during dusk (median depths day/dusk: 180.0 m/165.1 m) which is reflected in the measurements of altitude (median height day/dusk: 14.3 m/29.8 m). At night herring are observed in two primary modes, a shallow mode near 40 m and one within 30 m of the seafloor. During dawn the shallow mode is reduced and deepens to around 100 m while the deep mode is observed near 40 m above the seafloor. Non-herring schools have a bi-modal distribution for all time periods with the deep mode within 30 m of the seafloor and the shallow mode within 40 m of the ocean surface.

Distributions of fish aggregation sizes (lengths and thicknesses) are illustrated for both day and night observations (Fig. 9). Herring school lengths have a peak in the distribution near 60 m (day) and 30 m (night) compared with a more uniform distribution between 30 and 160 m for the non-herring schools that is similar for both day and night. All of these distributions have a long tail out beyond 500 m in school length. The school thickness distributions are similar in all cases with a sharp peak near 4 m except for the night distribution of herring which are distributed more uniformly between 4 and 11 m.

An important parameter for acoustically modeling aggregations of scatterers is their numerical density shown for observed fish schools composed of Atlantic herring at both day and night (Fig. 10). Observed volume backscattering strengths of the schools were used to derive fish school densities, ρ_s from Eq. (2):

$$\rho_s = \frac{10^{S_V/10}}{\bar{\sigma}_{\mathrm{bs}}}, \tag{3}$$

where the average differential backscattering cross section from Eq. (1), $\bar{\sigma}_{\mathrm{bs}} = \langle 10^{\mathrm{TS}/10} \rangle$, is estimated using observed length distributions from combined trawl hauls over all depth sampled. The brackets in this case represent an average over the observed length distribution. A depth-dependent regression of target strength of Atlantic herring averaged over their *in situ* tilt-angle distribution (i.e., the angle between the longitudinal axis of the fish body and the horizontal) is given by Ona.[32] This regression (all in m) is based on total fish length, L_{TL}—the straight-line distance

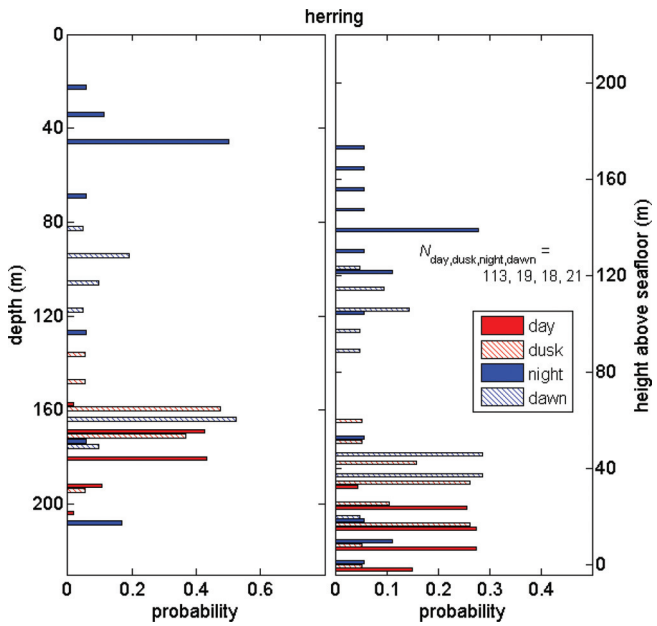

FIG. 7. Atlantic herring depth distributions (left panel) and height-above-seafloor distributions (right panel) derived from measurements of a downward-looking, multi-frequency echosounder from the FRV *Delaware II*. Data are divided into time periods of day (red), dusk (red hashed), night (blue), and dawn (blue-hashed).

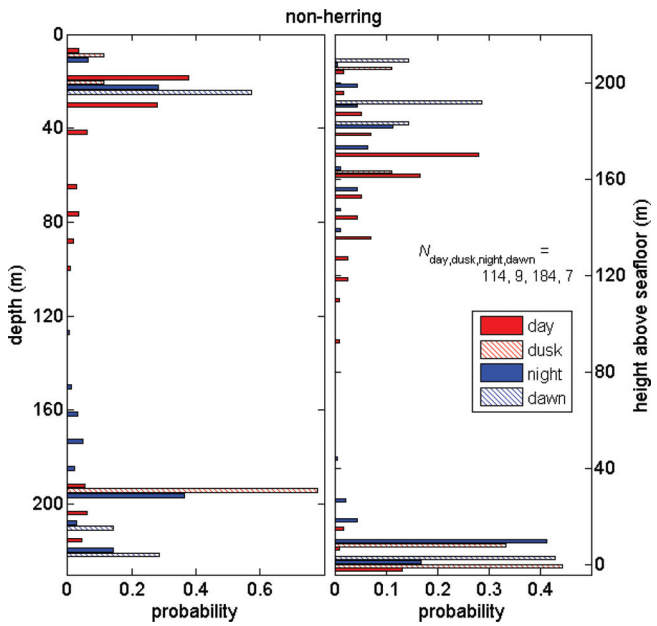

FIG. 8. Depth distributions (left panel) and height-above-seafloor distributions (right panel) of fish other than Atlantic herring derived from measurements of a downward-looking, multi-frequency echosounder from the FRV *Delaware II*. Data are divided into time periods of day (red), dusk (red hashed), night (blue), and dawn (blue-hashed).

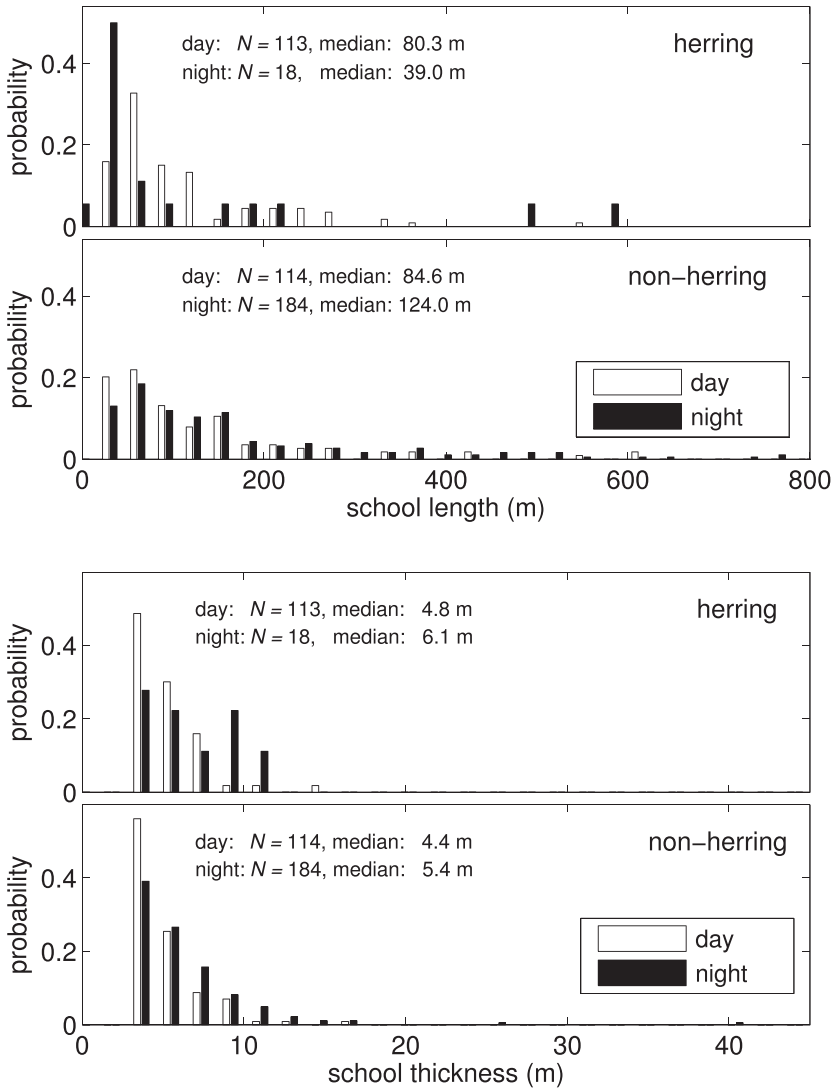

FIG. 9. Normalized histograms of fish school characteristics (length—top panels, mean thickness—bottom panels) derived from day and night measurements of a downward-looking, multi-frequency echosounder from the FRV *Delaware II*. Data are divided into Atlantic herring and non-herring schools. Length distributions are truncated at 800 m and a single herring thickness outlier at 84.3 m in the night data are not shown to better display results. Total numbers of schools observed, N, and median values are given in each panel.

from the tip of the snout to the end of the longest tail fin, and depth, z, given as

$$\mathrm{TS} = 20\log_{10}(100L_{\mathrm{TL}}) - 2.3\log_{10}(1 + z/10) - 65.4. \tag{4}$$

Fork length, L_{FL}, the distance from the snout to the middle of the caudal fin for forked-tail species, was the parameter measured in this experiment. The relationship to total length of Atlantic herring is given by $L_{\mathrm{TL}} = 1 \times 10^{-4} + 1.103L_{\mathrm{FL}}$.[33]

B. Biological sampling

Trawls were conducted on an *ad hoc* basis from the FRV *Delaware II* in order to sample fish when they were observed acoustically with the downward-looking echosounder. Of the 11 trawls used in this analysis, four were conducted during the day and seven were conducted at night. Three species, Atlantic herring, silver hake (*Merluccius bilinearis*), and Acadian redfish (*Sebastes fasciatus*) comprised most of the trawl catches. Herring and hake were caught at all depths sampled (mean depths: 107.4–198.5 m) during both day and night with small hake caught in the highest abundance (mean fish per trawl: $\bar{\mathrm{N}}_{\mathrm{herring}} = 161.3$, $\bar{\mathrm{N}}_{\mathrm{hake}} = 463.9$). Redfish were only caught in significant quantities (>20 fish/trawl) at night at deep depths (170.1–198.5 m) with a mean number in these trawls of $\bar{\mathrm{N}}_{\mathrm{redfish}} = 134.8$. The fork lengths of silver hake and Atlantic herring were narrowly distributed about means of 4

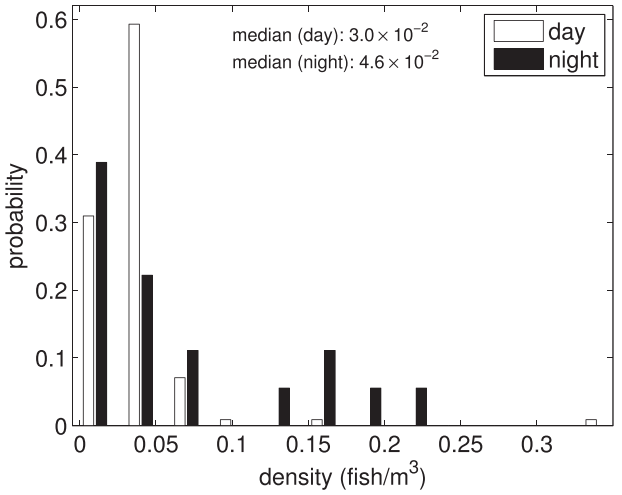

FIG. 10. Normalized histograms of Atlantic herring density within schools derived from day (white) and night (black) measurements of a downward-looking, multi-frequency echosounder from the FRV *Delaware II*.

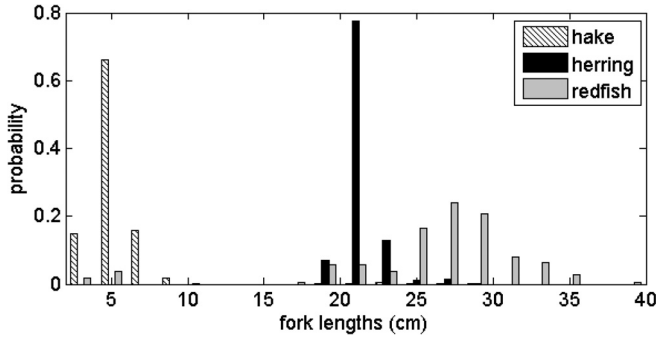

FIG. 11. Normalized fork length distributions of three species of fish caught in trawls from FRV *Delaware II*: silver hake (black-and-white hashed), Atlantic herring (black), Acadian redfish (grey). There are trace probability values of silver hake between 19 and 29 cm.

and 21 cm, respectively; while, Acadian redfish had a broad distribution of lengths between 18 and 39 cm, with a small percentage below 10 cm (Fig. 11).

C. Classification of broadband, long-range echoes

Long-range echoes are characterized both spectrally and temporally to aid in discriminating between echoes from aggregations of fish and echoes from other sources. Data associated with LFM1 (Table I) are georeferenced and compared with acoustic propagation predictions. Data associated with the broader bandwidth waveform, LFM2 (Table I), are analyzed for spectral clues characteristic of resonant swimbladder-bearing fish. Four sets of data were formed from contiguous regions where there were many fish-like echoes (Table III). The regions, defined by a narrow range of receiver beams and transmission times, produce sets of echoes that, locally, are assumed to be both spatially and temporally stationary. For the spectral analysis, two-way travel time was limited to 2–9 s (∼1.5–6.5 km range to scatterers).

1. Spatio-temporal analysis

Georeferenced echoes observed by the long-range sonar are illustrated in four examples (Fig. 12). The echo data are overlaid with predicted annuli of the refracted acoustic beam near the deep turning points—propagation paths illustrated in Fig. 13—as they intersect the observed depths of herring determined from downward-looking echosounder data (Fig. 7). A large portion of the received long-range echoes, presumed to be compact schools of fish are located within these annuli. In addition, a significant portion of the echoes fall well outside these annuli indicating fish at a shallower depth or fish ensonified outside of the main beam. Note that the left–right ambiguity in the HLA data about the ship heading is unresolved. However, the combination of the height above the bottom where most fish were observed in

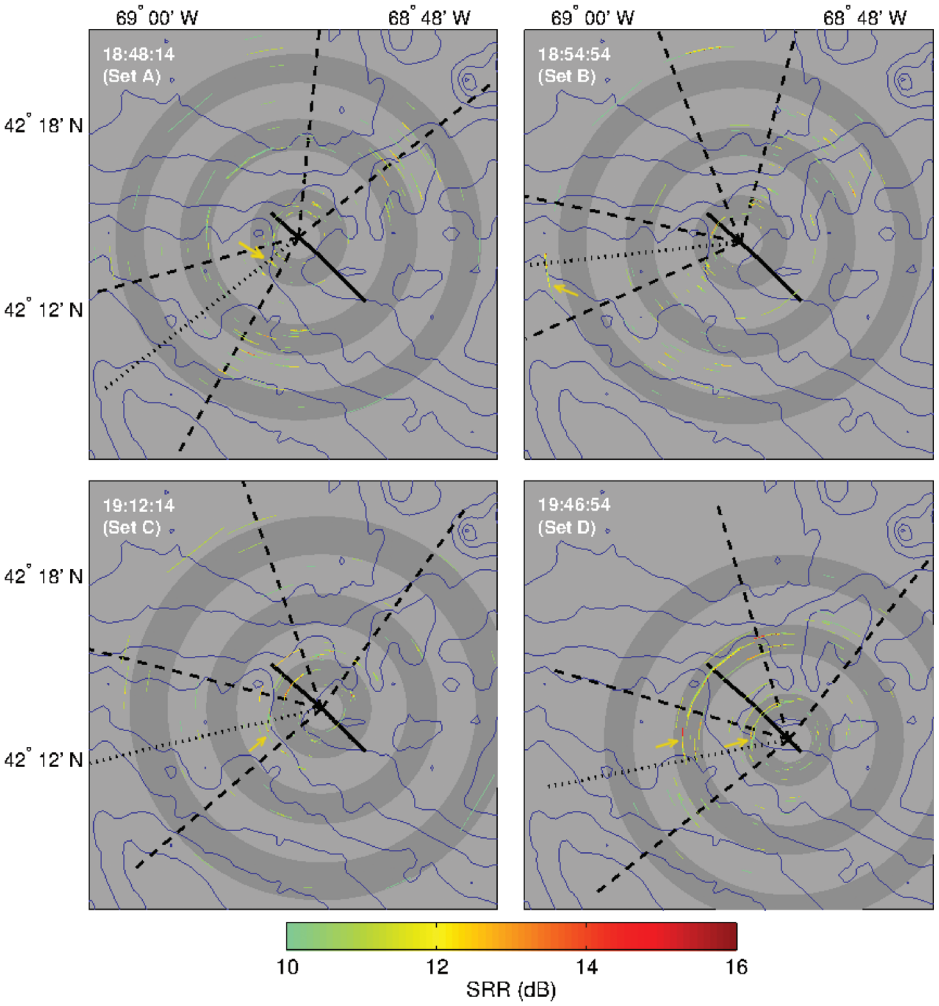

FIG. 12. Cruise track of RV *Oceanus* from 2221 to 2359Z on September 11, 2011 (black solid lines) and bathymetry contours (blue lines) corresponding to the same regions displayed in Fig. 6. Peaks (>10 dB) of single ping, normalized time-series measured by horizontal-looking sonar overlayed with −3 dB HLA beam limits (black dashed lines). Data are georeferenced using minimum mean sound speed observed in the region (see Fig. 3). Beam limits correspond to single-ping beam-space analyzed for given data set. Darker grey concentric rings show intersection of deeper refracted acoustic path with depths where herring were observed in echosounder data (see Fig. 13). Arrows indicate examples of fish likely located in the lower refracted paths (A and D) and higher in the water column (B and C). Transmission time and data set are indicated in top left of each panel.

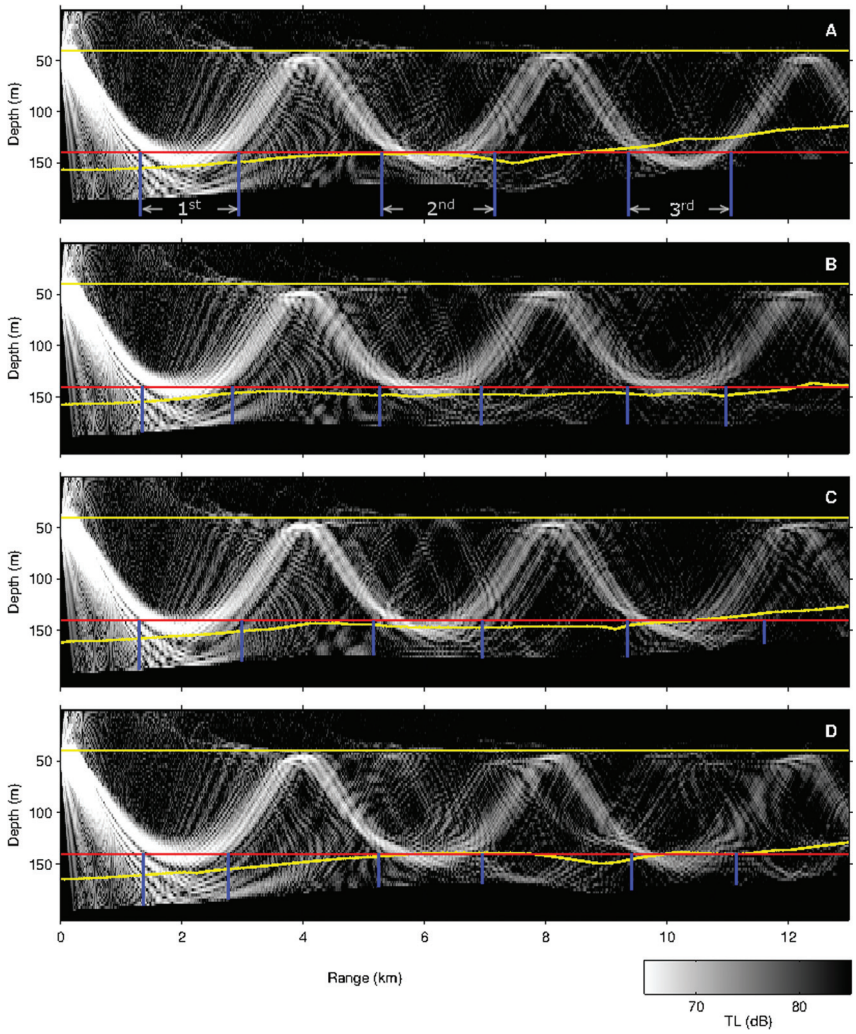

FIG. 13. Predicted transmission loss of long-range sonar signal along transects indicated by black dotted lines in Fig. 12 for data sets A–D. Non-herring were generally observed above 40 m depth or within 30 m of the bottom in downward-looking echosounder data as indicated by yellow lines. Red lines indicate depth (140 m) below which herring were observed in echosounder data during periods of day and twilight. Blue lines indicate boundaries of intersections between herring-observed depths and 1st, 2nd, and 3rd deep-refracted acoustic paths corresponding to the inner, middle, and outer dark-grey rings in Fig. 12. Modeling parameters are provided in Table II.

the downward-looking echosounder data (Figs. 7 and 8) and the maximum depth that the horizontal-looking sonar ensonified (Fig. 13) suggests that most echo returns emanated from the Franklin Swell region. Furthermore, modification of the ship's heading throughout the survey helped localize the sources of the vast majority of the high SRR echoes to this area (data not shown). The incorporation of internal-wave-induced perturbations had little effect on the placement of the primary acoustic paths except for a slight spreading of the annuli at the deep turning point.

2. Spectral analysis

High amplitude echoes (SRR ≥ 15 dB) were analyzed for spectral content as described in Sec. IV B. Calculations of acoustic resonance responses were made using the Love swimbladder scattering model [Eq. (A1)] applied to mixed assemblages of fish and compared with the observed spectra (Fig. 14) to classify the sources of scattering. In the observed data, the combination of source shading (Table I), a monotonically decreasing source level with decreasing frequency below 3.5 kHz, and the 6-dB SNR threshold results in a varying degree of truncation at the low-end of each spectrum. A combination of published and empirical parameters relating to the fish were used in this model, with the parameters directly related to the Love swimbladder given in Table IV. The coefficient for the regression of the swimbladder volume to the fish length, A in [Eq. (A2)], and the viscosity of fish flesh, ξ, are published parameters for the same species in all cases except for Acadian redfish larger than 12 cm. Since there are no published parameters available for this physoclist species, ξ for silver hake, also a physoclist species, was used in these predictions. The term A, though, was determined by a fit to the data as the frequency of the resonance peak is highly sensitive to this regression coefficient.

In order to verify that the deduced value of A was reasonable for redfish, comparisons were made with known values for silver hake. It is known that Acadian redfish are larger bodied than silver hake; and, data from NOAA-NEFSC (Ref. 34) show that, in a comparison of 20 cm long Acadian redfish and silver hake, the ratio of their masses is approximately 2.4. For a fish in a state of neutral buoyancy it is assumed that the volume of the swimbladder, and thereby A by Eq. (A2), is directly proportional to the mass of the fish. Multiplying A for large silver hake by this factor gives an estimated A for redfish of 6×10^{-5}. Fitting the model to the data resulted in a value of A for redfish of 1×10^{-4} within an order of magnitude of the estimate.

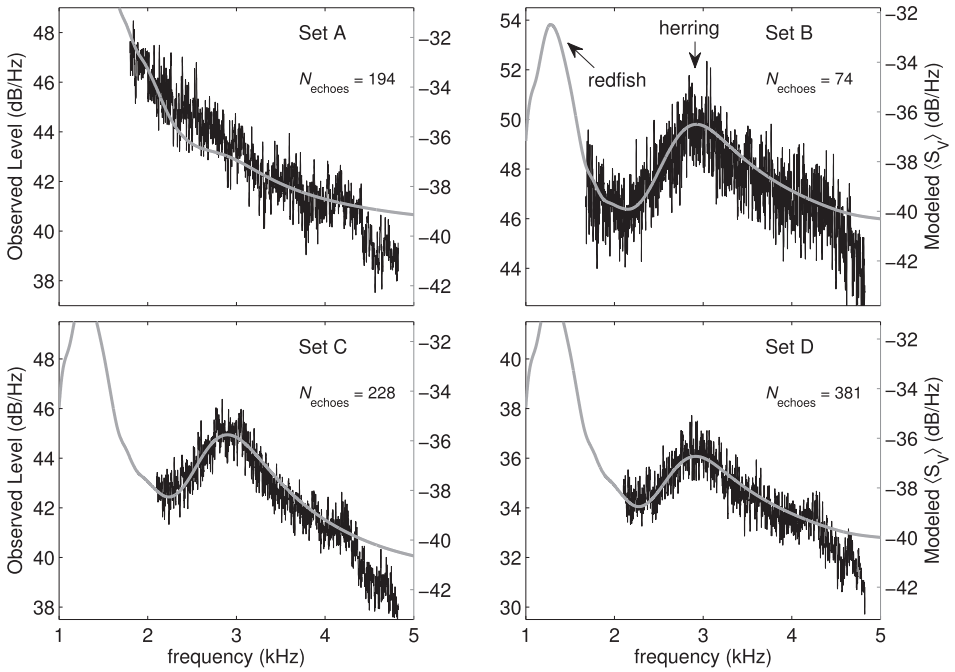

FIG. 14. Four sets of observations (black) of volume backscattering strength spectra compared with best-fit mixed assemblage model (grey). Observed data are averaged, match-filtered data over N_{echoes} spectra (number given in top right of each panel). Observed levels vary from set to set due to variation in transmission loss and beam location. Model predictions are average volume backscattering strengths of a mixed assemblage of silver hake, Atlantic herring, and Acadian redfish with relative densities given in Table V. Key modeling parameters of the underlying resonant scattering model are given in Table IV. Arrows indicated resonance peak in model and data (when in source band) of given species.

The depth of the fish was determined by fitting the main resonance peak near 3 kHz in the observed data (Fig. 14—sets B, C, and D) as described in IV B. Both single-valued depths and ranges of depths were considered. This analysis was simplified by the unimodal length distribution of each species resulting in a predicted frequency response with a single peak within the measured band. A single-valued depth of 146 m was determined through this approach and is within the range of trawl depths at which the three species were caught (107.4–198.5 m for silver hake and Atlantic herring, and 133.2–198.5 m for Acadian redfish).

The maximum relative density contribution comes from Atlantic herring in three of the four cases (B, C, and D). The predicted resonant scattering by these fish produce the spectral peak near 3 kHz which is observed in these three data sets. The predicted spectral peak near 1.5 kHz is from resonance scattering by larger Acadian redfish. Two data sets (A and B) appear to show a rise with decreasing frequency below 2 kHz that agree with the redfish resonance prediction. Finally, although the resonance peak for the much smaller silver hake occurs above 5 kHz and is therefore not seen in the data, the inclusion of this species in the model reduces the magnitude of the slope above 3.5 kHz and produces a better fit with the data.

D. Echo statistics

The statistics of observed high-amplitude echoes (SRR $\geq$ 15 dB) are examined from three sets (B, C, and D) of long-range, horizontal-looking sonar data, and then compared with theory and simulations. Broadband echoes from these beam-time regions are shown to have a spectral peak near 3 kHz (Fig. 14) suggestive of echoes dominated by Atlantic herring near this frequency. The echoes analyzed in this section correspond with transmissions of LFM1 (Table I). Two primary effects are examined: the range dependence of the echo-envelope PDFs and the effects of the directional beampattern on the echo statistics. Predictions of the echo statistics are also made using the phasor-summation method and compared with the data.

1. Range-dependent statistics

To determine if the echo envelope distributions have a range dependence, echoes from sets B, C, and D (Table III) are grouped into range bins of width ~500 m over the ranges ~1.5–11.9 km. Bins with 15 or more echoes were considered for analysis. Of the 23 range bins, 10 bins contained more than 15 echoes, N_{echoes}, with an SRR of at least 15 dB, with no range bins beyond 8 km meeting this threshold. Within

TABLE IV. Resonant swimbladder scattering model parameters. The coefficient of the regression of swimbladder volume from fish length, A, and the viscosity of fish flesh, ξ, are published parameters in all cases except A for large Acadian redfish which is obtained by fits to the data. Fish depth, z, is 146 m in all cases.

	Atlantic herring[a]	silver hake ($L < 12$ cm)[b]	silver hake ($L > 12$ cm)[c]	Acadian redfish ($L < 12$ cm)[b]	Acadian redfish ($L > 12$ cm)[d,e]
A	5×10^{-4}	5×10^{-4}	2.5×10^{-5}	5×10^{-4}	1×10^{-4}
ξ (Pa · s)	80	5	30	5	30

[a] A and ξ are published parameters for 25 cm Atlantic herring at 182 m depth (Ref. 18).
[b] A and ξ are published parameters for "small mixed" fish at 82 m depth (Ref. 18).
[c] A and ξ are published parameters for silver hake at 55 m depth (Ref. 18).
[d] ξ is a published parameter for silver hake at 55 m depth (Ref. 18).
[e] A is obtained by fitting model to data sets A and B.

the individual sample windows, the temporal extent of the high amplitude echo was highly variable; therefore, each ensemble consists of a variable amount of the selected echo and background reverberation and noise. Echo PDFs were calculated from the data using the methods described in Sec. IV C with the total number of samples in each ensemble ranging from 2580 to 7623 samples. Representative examples are shown in Fig. 15. The echo envelope PDFs show very little range dependence over the ranges observed as indicated by the fixed parameter, $N = 1$, describing the predicted number of scatterers within the main lobe at all ranges.

2. Predictions of echo statistics with phasor-summation method

Predictions of echo PDFs are made using the method of phasor summation (Sec. III C), and then compared with data.

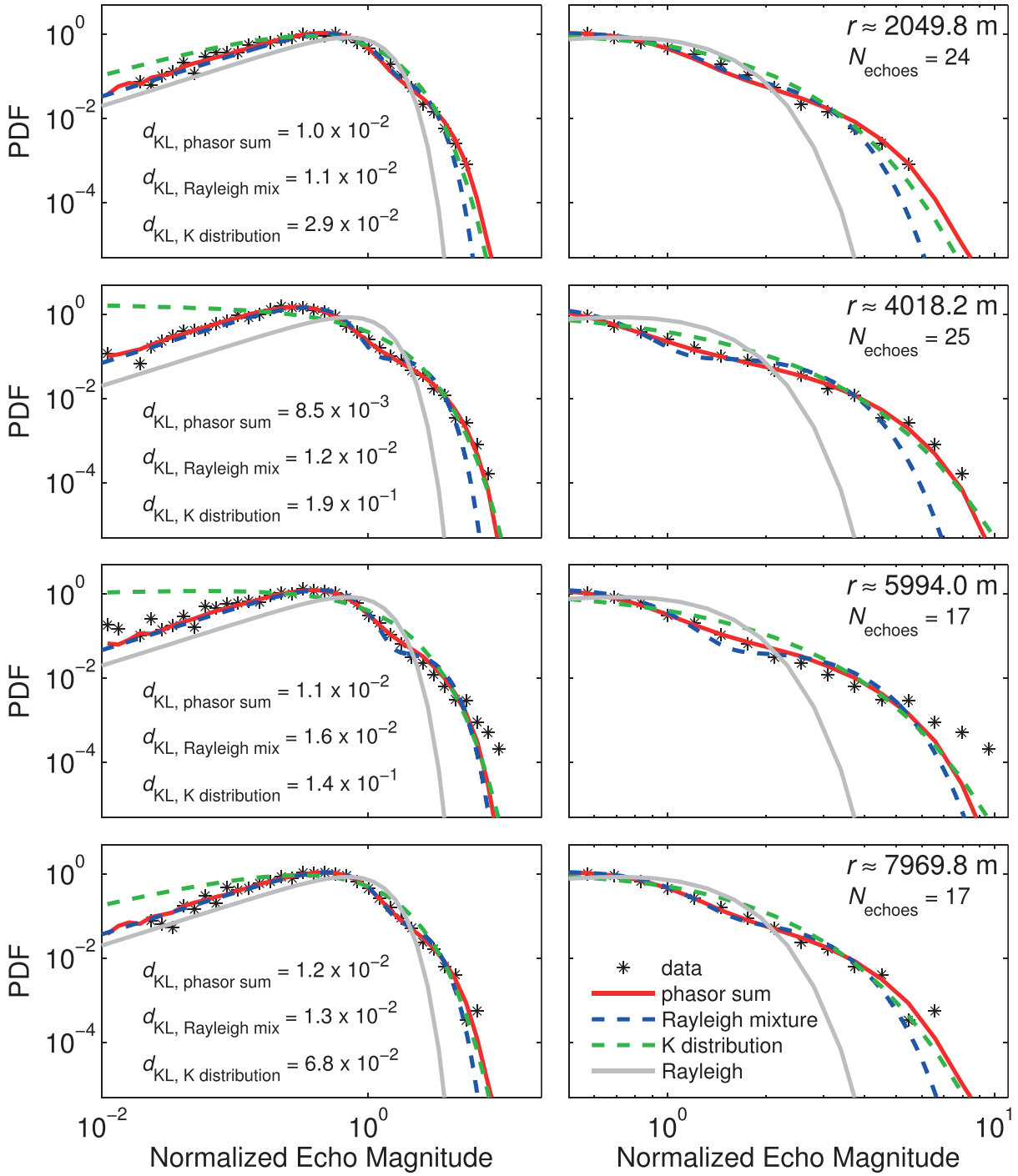

FIG. 15. Comparison of observed echo magnitude PDFs (black asterisks) for scatterers at various ranges from sets B, C, and D, compared with predictions by numerical phasor summation method (red solid), a two-component Rayleigh mixture (blue dashed), and the K distribution (green dashed). The Rayleigh distribution (grey solid) is provided for reference. Right panels expand the high amplitude tails of each distribution. The range, r, given in the right panels, is the approximate range to the beginning of a ~500 m range bin where echoes were measured. Results shown are limited to representative examples from the cases where the number of echoes in the ensemble, $N_{echoes} \geq 15$, (given in right panels). The Kullback–Leibler distances d_{KL} for the numerical phasor summation prediction (phasor sum), the two-component Rayleigh mixture (Rayleigh mix) and the K distribution, are given in the left panels.

The predictions are made at the center frequency 3750 Hz for a single scatterer, $N = 1$. The azimuthal beam angle, θ, was limited to $\pm\theta_{SL}$, where θ_{SL} is the angle at which the level of the main lobe decreases to the level of the highest side lobe (Fig. 5, top panel). The elevation angle, ϕ, was limited to the main lobe and first side lobe (Fig. 5, bottom panel). These parameters were kept constant for all ranges. Noise was added to the phasor summation and this parameter was varied for each range. Predictions are also compared with other PDF models that have been commonly used to characterize sonar echoes—the K distribution (see Ref. 23 and references within) and two-component Rayleigh-mixture distributions (e.g., Refs. 35–37).

With the exception of the high amplitude tail of the distribution at $r \approx 5994.0$ m, the phasor-summation predictions were in excellent agreement with the data at all ranges (see representative examples in Fig. 15). The K distribution, fit to the data using method of moments, generally fit the data well in the high amplitude portion except at this same range bin. The Rayleigh-mixture model, fit to the data using maximum likelihood estimation,[38] matched the data well in the low-amplitude region and near the inflection point, but consistently underestimated the probability in the tail of the distribution. The predictive phasor-summation model outperformed both empirically-derived distributions in all cases (see Kullback-Leibler distances, d_{KL} in Fig. 15) except for one range bin. In the single exception ($r \approx 5009.8$ m—not shown) the phasor summation and Rayleigh-mixture models performed comparably (d_{KL}, phasor summation/Rayleigh mixture $= 2.6 \times 10^{-2}/2.4 \times 10^{-2}$).

VI. DISCUSSION

A. Spectral classification of long-range echoes

In the data examined, echoes, measured by the broadband sonar system at long ranges, have spectral characteristics consistent with the presence of aggregations of swimbladder-bearing fish. A scattering model for mixed assemblages of fish shows that the spectral content of the echoes at these mid-frequencies can be reasonably represented by the resonant scattering of the three dominant species sampled in trawls during the experiment. Multiple scattering and resonance shifts have both been ignored as the observed fish schools do not meet the high packing density required to make these effects significant.[31] Most parameters used in the resonant swimbladder model are either published or observed values. Parameters that were unknown (i.e., those describing the swimbladder of large Acadian redfish) were fit to the data using reasonable values given known characteristics of these fish. A key observable used in the model was the length distribution of the individual fish. While this distribution was observed over a relatively large area that extends beyond the region coinciding with the long-range acoustic measurements, the length distributions are expected to be largely uniform at this time of year based on a series of annual NOAA surveys for the resident fish species in this part of the Gulf of Maine.[26]

An important parameter that is generally unknown when analyzing long-range sonar data is the depth of the scatterers associated with the recorded echoes. The single-valued depth of the fish applied in the scattering model (and derived from a fit with the observed data) results in predictions of a narrower resonance peak than if the scattering response was calculated for fish distributed over a range of depths (Fig. 14). There are at least two possible reasons why the data are consistent with these predictions. The first is that the fish ensonified in the analyzed data sets were distributed narrowly near the assumed depth and that the trawl samples, widely distributed over time and space, do not provide a good estimate of the distribution of fish for a narrow region in time and space. A second, more plausible, explanation is that the fish are more broadly distributed in depth, but echoes from fish located near the assumed depth dominate the mean spectra. This second explanation is reasonable because the echoes used in the spectral analysis are not corrected for transmission loss, an unknown quantity given the unknown depth of the scatterers. Without normalizing for variation in transmission losses associated with scatterers located in different parts of the waveguide, the mean spectra are likely biased by high amplitude echoes that arise when the fish are located at short ranges and in an energetic portion of the waveguide. These energetic regions can have a narrow extent in depth. For example, the region centered at a range of approximately 2 km is energetic very near the inferred depth of 146 m with an extent of 15 m (see Fig. 13, all panels). This propagation effect would give echoes associated with scatterers at these depths a stronger weighting in the mean spectra.

Another important unknown parameter in the spectral modeling was the relative numeric density of each species. While the trawl data provide some information on the dominant species present, no information regarding the relative masses of the species can be gleaned from these data for several reasons. The most significant reason is that it is impossible for any trawl to completely and properly sample and, hence, provide ground truth for a 24-km-diameter region that the long-range sonar ensonifies instantaneously. The trawl sampling was therefore conducted in such a manner to characterize what was *generally* present in the region, rather than to validate each and every sonar echo. In addition, there is inherent bias in samples collected by the trawl as the various species and sizes of fish sampled have different avoidance and selectivity rates for the trawl. Due to these limitations, the relative densities of each species were used as sliding parameters in fitting the modeled spectra to the acoustic data (Table V).

B. Echo statistics

Echoes, inferred to have arisen from compact aggregations of resonant swimbladder-bearing fish, are shown to

TABLE V. Relative densities of various species of fish used in mixed-assemblage spectral modeling of echoes from aggregations of fish.

Set	silver hake	Atlantic herring	Acadian redfish
A	0.00	0.15	0.85
B	0.28	0.57	0.15
C	0.05	0.69	0.26
D	0.28	0.46	0.26

produce highly non-Rayleigh envelope PDFs. These echoes that contain contributions from thousands of unresolved fish are presumed to have Rayleigh-distributed envelopes before beampattern effects. However, when the random locations of the aggregations within the beam are unknown, the random modulation of the echo by the beampattern cannot be removed and leads to a predictable distortion of the echo statistics. This effect has been shown in previous theoretical and experimental studies.[24,39] One major effect of the beampattern is to raise the high-amplitude portion of the echo-magnitude PDF above that of a Rayleigh PDF.[16,40] The non-Rayleigh tails of the echo PDFs observed in the data are attributed to this beampattern effect as evidenced by the close agreement with the phasor-summation model (Fig. 15). The low-amplitude portions of the echo-magnitude PDFs are also elevated and non-Rayleigh. This is primarily due to interfering system and ambient noise (not subject to beampattern effects). Finally, the mid-amplitude portions of the PDFs have an inflection which signifies the cross-over between noise-dominated and fish-dominated echoes.

Additionally, the distributions of echo envelopes were nearly invariant in range. Specifically, the high amplitude tails of the PDFs showed little range dependency, while the low amplitude portions, influenced heavily by noise, did show some variability. The stability of the statistics with range is most likely due to a combination of factors. First, the sparse spatial distribution of scatterers ensures that the number of unresolved aggregations in a given echo is no more than one over the observed ranges; and, second, the statistics of the pressure field is likely saturated over these ranges by natural randomness in the waveguide. These two factors result in a nearly constant distribution of normalized echo envelopes with range. Interestingly, the waveguide-influenced beampattern effects also remain constant, at least over the ranges analyzed.

It is expected that the invariance of the statistics with range would not apply at short ranges and in regions where the fish aggregations are more densely distributed. At short ranges the statistics of the pressure field will vary widely before reaching saturation (e.g., see Ref. 16). Additionally, the effect of the elevation-dependent component of the narrow beam may vary with range closer to the source where higher modes decay rapidly with range. Finally, for more densely distributed fish schools, the number of unresolved aggregations contributing to each echo is likely to vary with increasing sonar sample volume that increases as the square of the range. While all of these effects could add range dependencies to the echo statistics, the latter effect—which should be most significant at long ranges, could be explicitly accounted for in the phasor-summation model by making N a function of range given a known, or assumed, spatial density of fish aggregations.

It has also been shown that a physics-based model using a simple phasor summation can accurately predict the distribution of echo envelopes. The model accounts for (1) the number of unresolved schools in the sonar beam (at a given range), (2) the stochastic scattering response of the fish aggregation (i.e., a complex-Gaussian scattering response), (3) the beampatterns (both source and receiver) of the active sonar system, and (4) background noise and/or reverberation. The only sliding parameters used in the predictions were the limiting angles of the elevation-dependent beampattern and the noise level. Importantly, the inclusion of the beampattern in the model correctly predicted the location of the inflection point in the observed data, while the addition of noise had the primary effect of changing the slope of the low-amplitude end of the PDF.

Comparisons with the K distribution and a two-component mixed Rayleigh distribution show favorable comparisons over some portions of the distributions. Furthermore, it is expected that a K-Rayleigh mixture (e.g., see Ref. 41) would offer an improved fit by accounting for both the low-amplitude, Rayleigh-distributed noise and high-amplitude (i.e., K-distribution fitted) beampattern-influenced echoes. However, there are several pitfalls associated with this approach. First, the K distribution is non-predictive as it does not explicitly account for beampattern effects. Second, mixture models treat the distribution as a linear summation of two distinct sample volumes (i.e., an incoherent summation); whereas, real echoes contain noise that coherently interfere with the signal. Importantly, these issues can lead to inferred parameters, such as the relative proportion of noise and high-amplitude echoes, that are unrealistic.[42] In contrast, predictive models such as the phasor-summation model, in which the physical basis of each parameter is well understood, may be used to accurately infer information about the abundance and distribution of scatterers from which the echo statistics arise.

VII. CONCLUSION

This research is relevant to two widely disparate areas—fisheries research and sonar operations to detect scatterers other than fish in the water column where the presence of fish degrade system performance. For fisheries research, this study shows the potential for a high-resolution broadband sonar to spectrally classify echoes from fish, instantaneously, at long ranges. Such classification also aids in discriminating fish echoes, whose spectra are related to the swimbladder resonance, from echoes of non-biological entities, and in estimating important fish parameters such as density. The work also further emphasizes benefits demonstrated in previous long-range studies involving narrowband signals: (1) the ability to rapidly survey a large volume of water, and (2) the ability to measure sparse distributions of fish which may be under-sampled by nets or downward-looking echosounders.

As with prior studies involving long-range narrowband systems, challenges associated with these broadband sonar surveys include (1) non-uniform sampling of the water column in depth due to the coupling of a directional (depression-elevation dependent) sonar beampattern and the naturally refractive waveguide, (2) difficulties in inferring the depth of the aggregations (in the absence of contemporaneous downward-looking echosounder measurements) which is complicated by the combined fish length and depth dependencies of the scattering response of swimbladders, and (3) contamination of data from sources of scattering other than swimbladder-bearing fish (e.g., rocky outcroppings, non-swimbladder-bearing fish, marine mammals, etc.)—a

challenge that this study helps address through spectral analysis and associated classification/discrimination of scatterers. Finally, to reap the benefits of such surveys, it is clear that careful analysis of the data through realistic modeling of acoustic propagation is required.

From the standpoint that fish can be a source of clutter to an active sonar system, this study quantifies several important characteristics of echoes from aggregations of fish in shallow water. At mid-frequencies, 100-m sized aggregations of swimbladder-bearing fish can produce echoes with sufficient SRR to be observable above boundary reverberation in matched-filtered data. Furthermore, the distribution of echo envelopes from sparsely distributed aggregations, such as those observed near Franklin Swell in the Gulf of Maine, have highly non-Rayleigh (i.e., clutter-like) distributions of echo envelopes. Finally, a computationally inexpensive model has been shown to predict the distribution of the echo envelopes accurately. Since this physics-based model uses both sonar and fish parameters as input, it could potentially be used to help predict the probabilities of false alarm from fish aggregations in other regions of the world's oceans and using other types of sonars.

Future work related to this research may include developing population estimate techniques for surveying compact aggregations with a long-range, broadband sonar. With the capabilities for simultaneous classification and discrimination demonstrated through the use of broadband signals, spectral classification should be central to future survey techniques. Additionally, given the dependence of the echo statistics on the number of compact aggregations simultaneously ensonified, techniques could be developed to estimate the numbers of schools ensonified by a broadband, long-range system. Finally, by exploiting information on distributions of aggregation sizes, the aggregation number as inferred from echo statistics could, perhaps, provide a more robust parameter for inferring fish populations with a horizontal-looking system than direct calculation from volume backscattering strength in the absence of reliable depth information.

ACKNOWLEDGMENTS

This research was supported by the U.S. Office of Naval Research, the National Oceanographic Partnership Program, NOAA, WHOI, and the Oceanographer of the U.S. Navy. We would like to thank the science parties, officers, and crew of the research vessels *Oceanus* and *Delaware II*. We would also like to thank Richard Menis and Edward Kunz of NRL, Wendy Petersen of the Naval Undersea Warfare Center, Division Newport, and Cindy Sellers and Brian Guest of WHOI for their participation in the experiment.

APPENDIX: LOVE MODEL OF SCATTERING BY A RESONANT SWIMBLADDER

The Love model[43] is an empirically validated scattering model[19,28] that represents the swimbladder as a gas-filled, viscous, spherical shell. Following Nero *et al.*[28] the differential backscattering cross section as a function of depth and frequency is given as

$$\sigma_{\mathrm{bs}}(z,\mathrm{f}) = \frac{r_{\mathrm{eq}}(z)^2}{\left(\frac{\mathrm{f}_0(z)}{\mathrm{f}H(\mathrm{f})}\right)^2 + \left[\left(\frac{\mathrm{f}_0(z)}{\mathrm{f}}\right)^2 - 1\right]^2}, \tag{A1}$$

where $r_{\mathrm{eq}}(z)$ is the equivalent spherical radius at depth z and $\mathrm{f}_0(z)$ is the resonance frequency of the swimbladder.[28,32,43] For a fish of fork length L_{FL}, in m, the swimbladder volume at the surface, V_0, in m^3 is determined by regression of the fish length as

$$V_0 = A(100L_{\mathrm{FL}})^{3.35} \times 10^{-6}, \tag{A2}$$

where A is a dimensionless species-specific parameter given in Table IV. There are two major classes of gas-filled-swimbladder bearing fish: physoclists (e.g., silver hake and Acadian redfish), which maintain a constant volume of their swimbladder through gaseous exchange with their bloodstream; and physostomes (e.g., Atlantic herring), which are required to take in air at the surface. In the latter case, the volume of the swimbladder is subject to a change approximately following Boyle's Law when pressure changes with depth. The variation of the equivalent spherical radius of the swimbladder, r_{eq}, with depth is thus

$$r_{\mathrm{eq}}(z) = \begin{cases} r_0 & \text{physoclist} \\ r_0(P_0/P(z))^{1/3} & \text{physostome,} \end{cases} \tag{A3}$$

where r_0 is the radius of a sphere of volume V_0, P_0 is the ambient pressure at the surface, and P is the ambient pressure at depth z. From these dependencies, the resonance frequency, f_0, is shown to depend upon depth as $z^{1/2}$ and $z^{5/6}$ for the physoclists and physostomes, respectively.[28]

The term H in Eq. (A1) is a damping factor that includes damping due to acoustic radiation and viscosity while ignoring thermal damping. It is given by

$$H(z,\mathrm{f}) = \left(\frac{2\pi r_{\mathrm{eq}}(\mathrm{z})\mathrm{f}^2}{c\mathrm{f}_0(z)} + \frac{\xi}{\pi r_{\mathrm{eq}}^2(\mathrm{z})\mathrm{f}_0\rho_{\mathrm{f}}}\right)^{-1}, \tag{A4}$$

where c is a constant sound speed of 1500 m/s, ξ is the viscosity of fish flesh in Pa s given in Table IV, and ρ_{f} is the density of the fish flesh in $\mathrm{kg/m}^3$.

[1]D. E. Weston, "Fish as a possible cause of low-frequency acoustic attenuation in deep water," J. Acoust. Soc. Am. **40**, 1558 (1966).
[2]D. E. Weston and J. Revie, "Fish echoes on a long-range sonar display," J. Sound Vib. **17**, 105–112 (1971).
[3]J. S. M. Rusby, M. L. Somers, J. Revie, B. S. McCartney, and A. R. Stubbs, "Experimental survey of a herring fishery by long-range sonar," Mar. Biol. **22**, 271–292 (1973).
[4]D. E. Weston and H. W. Andrews, "Seasonal sonar observations of the diurnal shoaling times of fish," J. Acoust. Soc. Am. **87**, 673–680 (1990).
[5]D. M. Farmer, M. V. Trevorrow, and B. Pedersen, "Intermediate range fish detection with a 12-kHz sidescan sonar," J. Acoust. Soc. Am. **106**, 2481–2490 (1999).
[6]N. C. Makris, P. Ratilal, D. T. Symonds, S. Jagannathan, S. Lee, and R. W. Nero, "Fish population and behavior revealed by instantaneous continental shelf-scale imaging," Science **311**, 660–663 (2006).
[7]Z. Gong, M. Andrews, S. Jagannathan, R. Patel, J. M. Jech, N. C. Makris, and P. Ratilal, "Low-frequency target strength and abundance of shoaling Atlantic herring (*Clupea harengus*) in the Gulf of Maine during the Ocean

Acoustic Waveguide Remote Sensing 2006 Experiment," J. Acoust. Soc. Am. **127**, 104–123 (2010).
[8]R. C. Gauss, J. M. Fialkowski, E. L. Kunz, R. Menis, T. K. Stanton, C. J. Sellers, and J. M. Jech, "Clutter variability due to fish aggregations: Mid-frequency measurements in the Gulf of Maine," in *Proceedings of the 3rd International Conference and Exhibition on "Underwater Acoustic Measurements: Technologies and Results,"* edited by J. S. Papdakis and L. Bjørnø (2009), pp. 459–466.
[9]J. M. Gelb, R. E. Heath, and G. L. Tipple, "Characterization of clutter by class in mid-frequency active sonar," in *Proceedings of the International Symposium on Underwater Reverberation and Clutter* (2008), pp. 303–310.
[10]J. M. Gelb, R. E. Heath, and G. L. Tipple, "Statistics of distinct clutter classes in midfrequency active sonar," IEEE J. Ocean. Eng. **35**, 220–229 (2010).
[11]B. R. La Cour and J. E. Hamann, "Dynamic modeling of discrete biologics for active sonar simulation," IEEE J. Ocean. Eng. **35**, 164–174 (2010).
[12]O. R. Smith, "The location of sardine schools by super-sonic echo-ranging," Comm. Fish. Rev. **9**, 1–6 (1947).
[13]J. D. Stockwell, T. C. Weber, A. J. Baukus, and J. M. Jech, "On the use of omnidirectional sonars and downwards-looking echosounders to assess pelagic fish distributions during and after midwater trawling," ICES J. Mar. Sci. **70**, 196–203 (2013).
[14]P. Brehmer, T. Lafont, S. Georgakarakos, E. Josse, F. Gerlotto, and C. Collet, "Omnidirectional multibeam sonar monitoring: Applications in fisheries science," Fish Fish. **7**, 165–179 (2006).
[15]N. C. Makris, P. Ratilal, S. Jagannathan, Z. Gong, M. Andrews, I. Bertsatos, O. R. Godö, R. W. Nero, and J. M. Jech, "Critical population density triggers rapid formation of vast oceanic fish shoals," Science **323**, 1734–1737 (2009).
[16]B. A. Jones, J. A. Colosi, and T. K. Stanton, "Echo statistics of individual and aggregations of scatterers in the water column of a random, oceanic waveguide," J. Acoust. Soc. Am. **136**, 90–108 (2014).
[17]T. K. Stanton and D. Chu, "Non-Rayleigh echoes from resolved individuals and patches of resonant fish at 2–4 kHz," IEEE J. Ocean. Eng. **35**, 152–163 (2010).
[18]T. K. Stanton, C. J. Sellers, and J. M. Jech, "Resonance classification of mixed assemblages of fish with swimbladders using a modified commercial broadband acoustic echosounder at 1–6 kHz," Can. J. Fish. Aquat. Sci. **69**, 854–868 (2012).
[19]T. K. Stanton, D. Chu, J. M. Jech, and J. D. Irish, "New broadband methods for resonance classification and high-resolution imagery of fish with swimbladders using a modified commercial broadband echosounder," ICES J. Mar. Sci. **67**, 365–378 (2010).
[20]V. W. Young and P. C. Hines, "Perception-based automatic classification of impulsive-source active sonar echoes," J. Acoust. Soc. Am. **122**, 1502–1517 (2007).
[21]S. M. Murphy and P. C. Hines, "Examining the robusteness of automated aural classification of active sonar echoes," J. Acoust. Soc. Am. **135**, 626–636 (2014).
[22]J. M. Fialkowski and R. C. Gauss, "Methods for identifying and controlling sonar clutter," IEEE J. Ocean. Eng. **35**, 330–354 (2010).
[23]D. A. Abraham, "The effect of multipath on the envelope statistics of bottom clutter," IEEE J. Ocean. Eng. **32**, 848–861 (2007).
[24]D. Chu and T. K. Stanton, "Statistics of echoes from a directional sonar beam insonifying finite numbers of single scatterers and patches of scatterers," IEEE J. Ocean. Eng. **35**, 267–277 (2010).
[25]J. M. Jech and W. L. Michaels, "A multifrequency method to classify and evaluate fisheries acoustics data," Can. J. Fish. Aquat. Sci. **63**, 2225–2235 (2006).
[26]J. M. Jech and F. Stroman, "Aggregative patterns of pre-spawning Atlantic herring on Georges Bank from 1999–2010," Aquat. Living Resour. **25**, 1–14 (2012).
[27]"U.S. Geological Survey East-Coast sediment analysis: Procedures, database, and GIS data," U.S. Geological Survey, Coastal and Marine Geology Program, 2005.
[28]R. W. Nero, C. H. Thompson, and J. M. Jech, "*In situ* acoustic estimates of the swimbladder volume of Atlantic herring (*Clupea harengus*)," ICES J. Mar. Sci. **61**, 323–337 (2004).
[29]M. D. Collins, "A split-step Padé solution for the parabolic equation method," J. Acoust. Soc. Am. **93**, 1736–1742 (1993).
[30]J. A. Colosi and M. G. Brown, "Efficient numerical stimulation of stochastic internal-wave-induced sound-speed perturbation fields," J. Acoust. Soc. Am. **103**, 2232–2235 (1998).
[31]M. Andrews, Z. Gong, and P. Ratilal, "Effects of multiple scattering, attenuation and dispersion in waveguide sensing of fish," J. Acoust. Soc. Am. **130**, 1253–1271 (2011).
[32]E. Ona, "An expanded target-strength relationship for herring," ICES J. Mar. Sci. **60**, 493–499 (2003).
[33]W. J. Overholtz, J. M. Jech, W. L. Michaels, and L. D. Jacobson, "Empirical comparisons of survey designs in acoustic surveys of Gulf of Maine-Georges Bank Atlantic herring," J. Northwest Atl. Fish. Sci. **36**, 127–144 (2006).
[34]S. E. Wigley, H. M. McBride, and N. J. McHugh, "Length-weight relationship for 74 fish species collected during NEFSC research vessel bottom trawl surveys, 1992–99," NOAA Technical Memorandum NMFS-NE **171**, 1–36 (2003).
[35]A. P. Lyons and D. A. Abraham, "Statistical characterization of high-frequency shallow-water seafloor backscatter," J. Acoust. Soc. Am. **106**, 1307–1315 (1999).
[36]T. C. Gallaudet and C. P. d. Moustier, "High-frequency volume and boundary acoustic backscatter fluctuations in shallow water," J. Acoust. Soc. Am. **114**, 707–725 (2003).
[37]N. P. Chotiros, "Non-Rayleigh distributions in underwater acoustic reverberation in a patchy environment," IEEE J. Ocean. Eng. **35**, 236–241 (2010).
[38]D. A. Abraham, "Modeling non-Rayleigh reverberation," Technical Report No. SR-266, SACLANT Undersea Research Centre, La Spezia, Italy, 1997.
[39]T. K. Stanton and C. S. Clay, "Sonar echo statistics as a remote-sensing tool: Volume and sea-floor," IEEE J. Ocean. Eng. **11**, 79–96 (1986).
[40]S. Bhatia, T. K. Stanton, and K. Baik, "Non-Rayleigh scattering by a randomly oriented elongated scatterer randomly located in a beam," IEEE J. Ocean. Eng. **40**, 169–176 (2015).
[41]D. A. Abraham, J. M. Gelb, and A. W. Oldag, "Background and clutter mixture distributions for active sonar statistics," IEEE J. Ocean. Eng. **36**, 231–247 (2011).
[42]W.-J. Lee and T. K. Stanton, "Statistics of echoes from mixed assemblages of scatterers with different scattering amplitudes and numerical densities," IEEE J. Ocean. Eng. **39**, 740–754 (2014).
[43]R. H. Love, "Resonant acoustic scattering by swimbladder-bearing fish," J. Acoust. Soc. Am. **64**, 571–580 (1978).
[44]NOAA National Geophysical Data Center, "U.S. coastal relief model" (2012).
[45]B. A. Jones, "Echo statistics of aggregations of scatterers in a random waveguide: Application to biologic sonar clutter," Ph.D. dissertation, Naval Postgraduate School (2012).